Aeroelastic Optimization of Composite Wind Turbine Blades using Variable Stiffness Laminates

Etana Ferede
Research Scientist
Rensselaer Polytechnic Institute
Troy, NY, US

Mostafa Abdalla
Associate Professor
Delft University of Technology
Delft,Netherlands

Farhan Gandhi
Professor
Rensselaer
Polytechnic Institute
Troy, NY, US

Gerard van Bussel
Professor
Delft University of
Technology
Delft,Netherlands

Johannes Dillinger
Research Scientist
German Aerospace
Center (DLR)
Goettingen, Germany

ABSTRACT

A variable stiffness composite optimization framework for wind turbine rotor blades is presented. The framework consists of a multi-fidelity approach for wind turbine rotor analysis, where both structural and aerodynamic constraints are considered during the optimization. The potential of twist coupled blades to regulate the power on stall controlled wind turbines is investigated by exploiting the characteristic of unbalanced laminates to induce twist coupling. A complete stiffness variation along the blade span is considered during the optimization, while using the cost of energy as the objective function. Results show that unbalanced laminates provide a greater capabilitiy (compared to balanced laminates) to reduce the cost of energy of stall controlled wind turbines by exploiting extention-twist and bend-twist coupling of composite blades.

INTRODUCTION

There is a growth in the energy consumption of the world, leading to rapid depletion of natural resources, such as fossil fuels. Added to that, the environmental impact of fossil fuels (e.g. global warming) makes a renewable source of energy a better alternative for power generation. Among renewable energy sources, generating energy from wind is becoming more popular.

Although the number of installed wind turbines is increasing rapidly, there are still many challenges ahead for making the cost of generating energy from offshore wind competitive with other energy sources. One method for making the Cost of Energy (CoE) from wind competitive is to reduce the operational and maintenance cost of wind turbines. The operational and maintenance cost of wind turbines may be reduced by eliminating, as much as possible, rotating components of the turbine which are prone to wear and tear. While the power on most modern wind turbines are regulated using blade root pitch control versus wind speed(above rated wind speed), an alternative way to regulate power is to use stall control scheme, thereby eliminating the need to use the pitch mechanism.

With recent advances in composite technology for tailoring the structural response of composite structures, it is possible to apply the technique to the conventional passive stall control scheme. Particularly, the use of twist coupling for regulating (passively) the angle of attack, thus also the torque and power of the wind turbine, shows a promise to design adaptive blades for stall regulated wind turbines, with improved performance in terms of power and load control, as well as in terms of cost reduction.

Earlier investigations towards incorporating twist coupling in wind turbines blades, where mainly focused on obtaining the theoretically maximum twist coupling that can be achieved using angled ply lay-ups. A review on twist coupled blades for enhancing the performance of HAWTs is provided in (Ref. 1), which includes all the research conducted in this field, prior to 2001.

Presented at the AHS International 73rd Annual Forum & Technology Display, Fort Worth, Texas, USA, May 9–11, 2017.

Among others, earlier work of Karaolis et al. (Ref. 2) investigates the potential gain of twist coupling to control the aerodynamic loading on wind turbines. Different coupling schemes were investigated that include bend-twist and extension-twist coupling. Furthermore, the amount of twist coupling gained by pressurizing the interior of the wind turbine blade is also investigated. However, the aerodynamic performance of the blade models was not assessed using wind turbine aeroelastic simulations, which makes the conclusions from this work on the possible twist coupling that can be achieved in wind turbine blades purely theoretical.

Similarly, several research papers (Refs. 3–5) are dedicated to finding the optimal fiber angle that maximizes the amount of twist coupling in composite blades. The research papers come to the same conclusion that fibers at 20 deg (with respect to the blade axis) result in maximum twist coupling. These research papers, however, do not assess, simultaneously, the effect of twist coupled blades on the aerodynamic performance of the wind turbine blades.

A few research papers are published that evaluate the aerodynamic performance of twist coupled blades by prescribing the amount of twist coupling during the aerodynamic simulation. For example, the work of Lobitz et al. (Refs. 1, 6) shows the potential of bend-twist coupled blades in enhancing energy extraction and reducing fatigue loads, while assuming a prescribed bend-twist coupling during the analysis.

Recent investigations towards twist coupled blades looks into the benefit of twist coupling using more reliable methods for calculating the aeroelastic response of the blades. Maheri et al. (Ref. 7) uses analytical/FEA coupled aeroelastic simulation of bend-twist coupled blade and assess the improvement in energy capture capability of a stall regulated wind turbine. However, the method does not consider span-wise variation of the (composite) laminate properties and also uses limited constraints during the optimization process. Especially, structural constraints such as stress distribution across the blade skin and buckling, as well as constraints on maximum tip deflection are not considered.

Alternatively, Maheri et al. (Ref. 8) proposed another method to design bend-twist coupled blades, were the structural and aerodynamic designs are carried out separately. The method incorporates the *induced* twist during the aerodynamic design, as part of the design parameters, while during the structural design, the material, and structural parameters are optimized that meet the *induced* twist requirement from the aerodynamic design. However, this method suffers from simplifying assumptions associated with decoupling the structural and aerodynamic design. Furthermore, detailed constraints (stress, buckling, tip deflection) were not considered during the optimization.

The works of Capuzzi et al. (Refs. 9–11), follow a similar approach as in (Ref. 8), where the aerodynamic and structural design of bend-twist coupled blades is performed separately. First, the 'target' twist curves for optimum power production is determined during the aerodynamic design (Ref. 9). The 'target' twist curves are parametrized in terms of the radial position and wind speed. Subsequently, a structural design is carried out that achieves the 'target' twist curves (Ref. 10). Furthermore, starting from the structural design of the adaptive blade in (Ref. 10), a detailed structural design, including strength and buckling constraints, is performed in (Ref. 11).

Bottasso et al. (Ref. 12) present a parametric design of bend-twist coupled blades for passive and a combination of passive-active method for load alleviation. To evaluate the level of bend-twist coupling, different blade designs are studied consisting of a single biased fiber angle (with respect to the blade axis), placed partially or fully along the blade span. A multidisciplinary optimization (MDO) procedure is then used to design the different blades, subjected to multilevel constraints.

A parametric study for load mitigation, using aeroelastic tailoring for maximum bend-twist coupling, is carried out in (Ref. 13). However, the method does not include any structural constraints (stress, buckling and tip deflection) during the parametric study.

Another method for inducing twist coupling in wind turbine blades is through geometric design. By designing a swept blade planform, the additional moment caused by the blade sweep twists the blade to stall or to feather depending on the direction of the blade sweep (Ref. 14). The design by Sandia (Ref. 15) demonstrates the benefit of swept blades for enhancing power capture, without increasing the thrust load.

Most of the research conducted so far is to investigate the benefit of twist coupled blades for power and/or load regulation; either based on a parametric study using few design variables or using simplified models for analyzing the aeroelastic response of adaptive blades. The next step would be to perform a detailed optimization study where the laminate properties are varied across the blade cross-section and along the blade-span. The goal is to investigate the increase in aerodynamic performance of stall controlled wind turbines using composite blades with variable stiffness along the blade span and cross-section. Detailed structural and aerodynamic constraints need to be included in the optimization study, while using an analysis tool with sufficient complexity to accurately capture the aeroelastic response of twist coupled blades.

This paper presents a variable stiffness composite optimization method for wind turbine rotor blades and investigates the benefit of using composite materials to design twist coupled blades for large scale (stall regulated) wind turbines. An isogeometric framework (Ref. 16) that unifies the parametrization of a wind turbine rotor blade and analyses its aeroelastic response is used in this paper. The framework consists of a multi-fidelity approach for wind turbine rotor analysis, where both the structural and aerodynamic responses are calculated using isogeometric analysis.

METHODOLOGY

The optimization framework presented here is intended for optimizing variable stiffness laminates used in the design of the structural components of wind turbine blades. The optimization process employed in this work corresponds to a successive optimization of convex local approximations of the

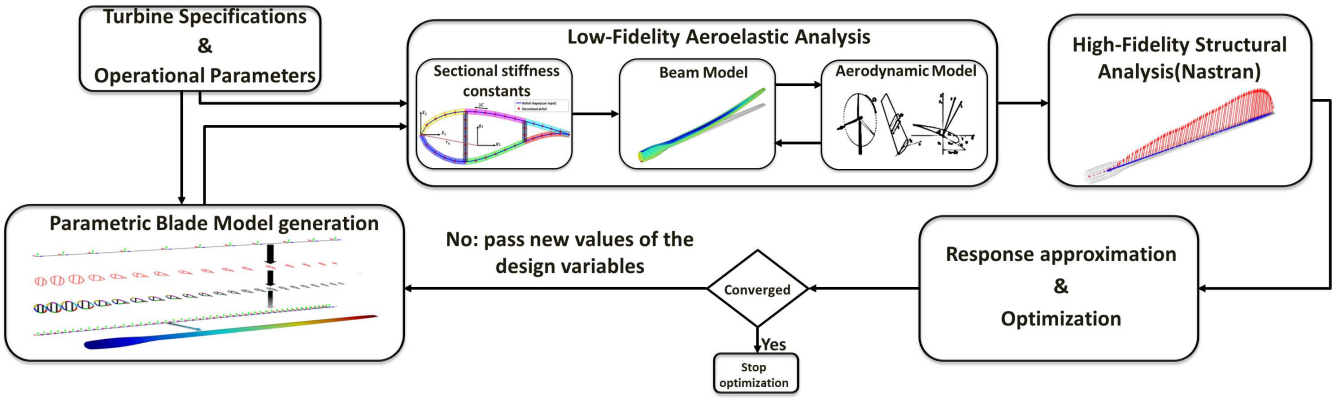

Fig. 1. Schematic overview of the optimization methodology

responses, using a gradient based optimizer. A schematic overview of the optimization framework is given in figure 1. Referring to figure 1, the optimization process follows two basic steps.

For the first step, starting from the initial design point and user supplied turbine specifications (Rotor diameter, blade planform, etc..) the sequence of generating the required responses and their sensitivities is divided in three tasks. First, the blade geometry, including its *FE* model, is generated based on the Isogeometric Analysis (IGA) principle. Isogeometric analysis is a computational approach that unifies finite element analysis with NURBS-based Computer Aided Design (CAD) method (Ref. 17). Non-Uniform Rational B-Spline (NURBS) representations are commonly used to construct descriptions of engineering products. Using the user supplied operational parameters (range of operational wind speeds, rotational speed, etc..) the loads on the turbine blade are calculated using a *low-fidelity* aeroelastic model, generating the aeroelastic responses and their sensitivities with respect to the design variables. The (*low-fidelity*) aeroelastic module is a one dimensional beam model, based on the *IGA* precept, to predict both the aerodynamic loads and the structural deformations. The aeroelastic loads are then applied, together with their sensitivities, as design dependent loads unto a *high-fidelity* finite element model. This is followed by detailed structural analysis, together with the sensitivity of the structural responses, using the *FE* solver *NASTRAN*.

In the second step, after generating the responses and their sensitivities, an approximation model, suitable for the chosen optimization tool, is formulated using both the responses and their sensitivities. The response approximations are then passed to the optimizer which iterates on the approximated model till the minimum that satisfies the constraints is found, resulting in new design variables. The new design variables are then passed to the analysis module and the whole process is repeated till the difference between successive optimum values of the objective function is below a given tolerance. In the next section, a brief description of the modules in figure 1 is given.

Turbine Specifications & Operational Parameters

This framework gets as input general turbine specifications, which are then used to model the geometry of the blade and define the turbine's configuration. The user supplied turbine specifications are: rotor radius, blade radius, hub radius, hub height, number of blades and blade planform data. The blade planform data consists of the chord and twist distribution along the blade radius. The hub height together with the wind speed at hub height is employed to calculate the wind shear profile, using the power law relationship. The wind shear profile is then used as input to analyse the average aerodynamic load on the blade, per blade rotation. Furthermore, the initial values of the design variables are provided.

In addition to the turbine specifications, operational parameters such as: cut-in, rated and cut-out wind speeds, together with the rated rotational speed and optimum tip speed ratio are used to determine the aeroelastic loads on the wind turbine blade. Since the framework takes into account the effect of wind shear, discrete sampling points of the azimuth angle are initially supplied to calculate the average aerodynamic loads on the rotor disc. Furthermore, the Weibull's probability density function for hub height wind speeds is supplied by the user to evaluate the annual energy production.

Parametric Blade Model generation

A parametric approach is set-up to model wind turbine blades with generic shapes including general airfoil shapes, planform, sweep or curvature of the centreline. The parametrization is intended to be used for performing parametric design studies and preliminary optimisation of the planform shape, blade axis, and material properties.

The blade geometry is modelled in the rotating, X_r, Y_r, Z_r frame, as shown in figure 3. The base vector e_2 is orthogonal to the rotor plane, while e_1, e_3 span the rotor plane. Moreover, a fixed frame is formed by the orthonormal triad E_1, E_2, and E_3, with the origin at the bottom of the tower. The position of the blade in the fixed frame is specified by the azimuth position ϕ, which is important in the calculation of the gravity load and wind shear effects.

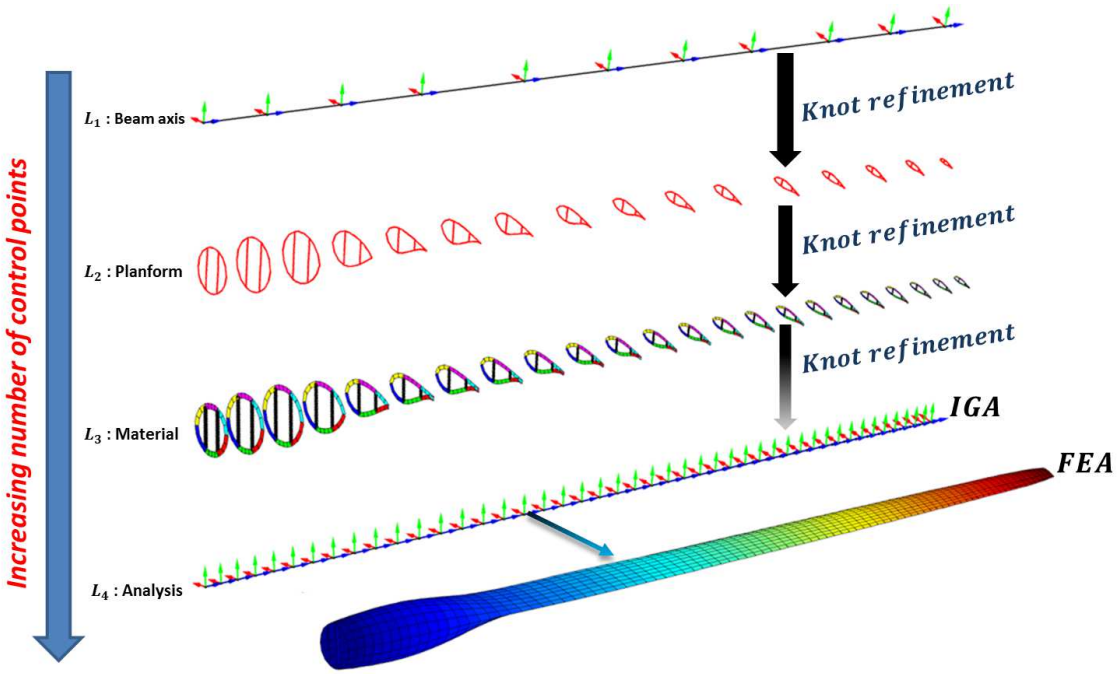

Fig. 2. Multi level parametrization of a wind turbine blade

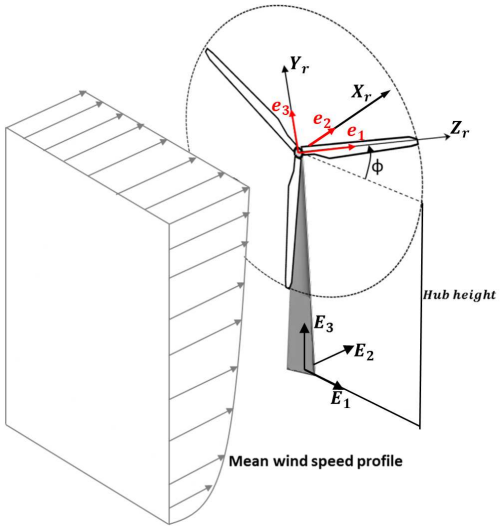

Fig. 3. Definition of moving reference frame and wind shear for wind turbine aeroelastic analysis

Blade geometry NURBS functions are used to parametrise the blade shape and material properties. A multi-level discretization scheme is used to parametrize the beam axis geometry, blade planform shape, and material distribution using successively finer control point nets as shown in figure 2. The mapping between different levels of refinement is performed using the *Knot refinement* method (Refs. 18, 19). Referring to figure 2, the beam axis is described as a 3D NURBS curve with the corresponding control points locations defined on the L_1 level. On the L_2 level, the cross-section variation (along the blade span) is parametrized by associating an airfoil geometry with each control point and interpolating using NURBS functions. The airfoil geometry associated with each control point is generated by a linear combination of pre-defined airfoil shapes. The orientation of each airfoil is defined by the local twist which is also represented by a NURBS function and control point nets on the L_1 level.

Material properties Composite laminates are used to define the material properties of a wind turbine blade. The laminate properties are described by a NURBS curve with the corresponding control point properties defined on the L_3 level. First, the laminate properties per control point are determined by dividing a cross-section in $N_{pr}+1$ sections, where N_{pr} laminates are assigned over the contour of a cross-section and a single laminate for the shear webs. A schematic representation of laminate assignment per cross-section is shown in figure 4, where 7 laminates are used to define the material properties over a cross-section. Symmetric laminates are used in the current optimization studies. Hence, the coupling matrix(B) is zero for all considered laminates. The laminate properties are comprised of the laminate thickness h, membrane stiffness matrix A, and bending stiffness matrix D. This brings to thirteen design variables per laminate: one variable for the laminate thickness, six variables for the membrane stiffness matrix and six variables for the bending stiffness matrix, exploiting the symmetric nature of the matrices.

FE model For the detailed structural analysis, the outer shape of the blade and the spars are modelled by shell elements. The properties of the shell elements are defined using laminate membrane and bending stiffness matrix and thickness. The geometry of the model and its Finite Element discretization remains unchanged during the optimization, ex-

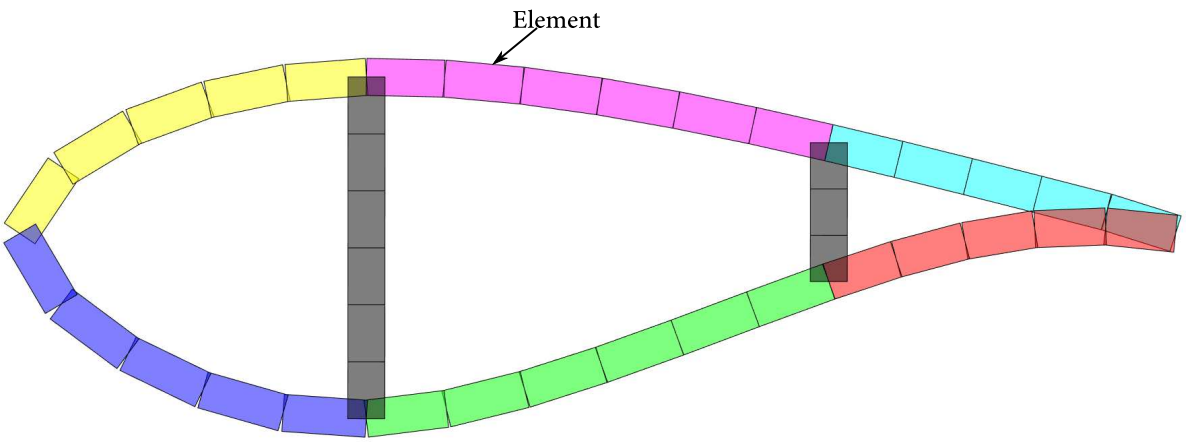

Fig. 4. Material property assignment over a cross-section, where each colour represents a single laminate.

cept the material properties, which are varied by the optimizer.

Low-Fidelity Aeroelastic Analysis

The next module in figure 1 (low-fidelity aeroelastic module) is used to calculate the loads on a wind turbine blade. It consists of three sub-modules that calculate: sectional (beam) stiffness constants, structural, and aerodynamic loads. The beam and aerodynamic sub-modules are coupled to calculate the aeroelastic loads on a wind turbine blade.

Structural model The wind turbine blade is modelled using isogeometric formulation of geometrically exact 3D beam theory (Refs. 19–21). The sectional stiffness constants, needed for the beam model, are calculated using an in-house tool (Ref. 22). Isogeometric formulation is used to descritize the solution space. Hence, the generalized coordinates for the displacement-based formulation consist of the control point quantity of the displacement and the rotation vector. In addition, gravitational and centrifugal loads are considered in the current framework.

Aerodynamic model The Blade Element Momentum(BEM) theory (Ref. 23) with tip loss correction (Ref. 24) is used to calculate the aerodynamic force and moment vector per unit length. In addition, a correction on the twist (observed by the free stream wind velocity) is added to account for the effect of blade flexibility. To apply this correction, it is assumed that the twist vary slowly along the blade span. Furthermore, wind shear is taken into account when calculating the aerodynamic loads on a single blade.

Aero-structural coupling For flexible structures, the aerodynamic loads are dependent on the structural deformation and vice-versa. The aeroelastic solution is obtained by equating the internal loads with external loads as:

$$R = f_s(q,u) - f_{ext}(q,u) = 0, \tag{1}$$

where R is the residual vector,f_s is the generalized structural load vector, q is the generalized displacement and rotation vector, and u is the incoming wind speed. The generalized external load vector (f_{ext}) is give by:

$$f_{ext} = f_a + f_g + \omega^2 \left(f_{cf} + K_{cf} q\right), \tag{2}$$

where ω is the rotational speed, f_a is the generalized aerodynamic load, f_g is the generalized gravitational load, f_{cf} is the generalized centrifugal load, and K_{cs} is the centrifugal stiffness matrix. Aeroelastic equilibrium is achieved when the residual converges to zero. The non-linear aeroelastic equilibrium is calculated by dividing the wind speed u into a given number of steps, controlled by the parameter λ, running from 0 to 1. At a given wind speed λu, a prediction of the equilibrium point for the next wind speed is made by linearising the equilibrium equation 1 around the current equilibrium point. Followed by a correction phase, keeping λ constant and varying the generalized coordinates p until the equilibrium equations in 1 are satisfied.

High-fidelity structural analysis

The next module in figure 1 performs detailed structural analysis of the wind turbine blade based on the aeroelastic loads calculated in the previous module. The finite element solver *NASTRAN* is used to perform detailed structural analysis, where the responses from *NASTRAN* are used to formulate the structural constraints that are passed to the optimizer. Both stress and buckling analysis are carried out by applying the aeroelastic loads, calculated using the aeroelastic module (as

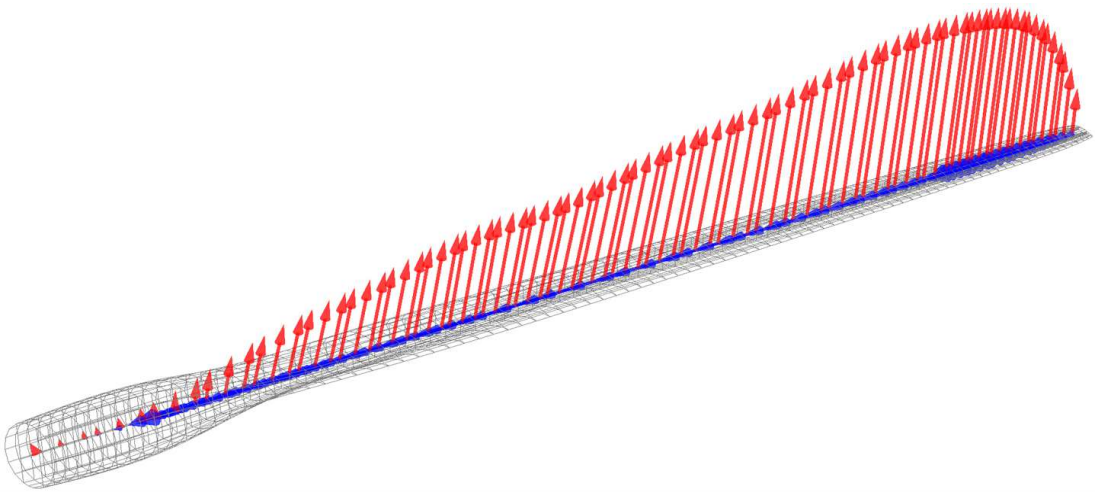

Fig. 5. Application of aeroelastic loads unto a finite element model (red = load distribution, blue = moment distribution)

design dependent loads) in *NASTRAN*. The aeroelastic loads consisting of: the aerodynamic, centrifugal and gravitational loads, are applied unto the *NASTRAN* model using the *RBE3* card. The *RBE3* cards are multi point connection elements used to (smoothly) introduce external loads to the finite element model. The aeroelastic force and moment resultants per unit length are interpolated on the *RBE3* elements using the principle of virtual work. Figure 5 shows a representation of applying the aeroelastic loads onto the finite element model for detailed structural analysis, where the red and blue arrows indicate the distributed force(including lift and drag) and moment resultants respectively. After applying the aeroelastic loads unto the *FE* model, the responses from stress and buckling analysis, together with the derivative with respect to the design variables are obtained from the *NASTRAN* analysis. The design optimization solution sequence is requested with the execution control statement *SOL 200*, while setting the parameter *END=SENS* of the *NASTRAN DSAPRT* card to halt *NASTRAN* analysis after generating the responses with their sensitivities.

Response Approximation & Optimization

In the final module of figure 1, the material properties of the wind turbine blade are optimized for a given objective function and constraints. A composite optimizer, based on lamination parameters, by IJsselmuiden et al (Ref. 25) is used. The design variables consist of the thickness normalized membrane and bending stiffness matrices, $\hat{A}$ and $\hat{D}$, together with the laminate thickness h.

The optimizer proposed in (Ref. 25) uses response approximations during the optimization. Therefore, linear approximation of the objective function and the constraints is formulated using *Taylor* series expansion of the responses in terms of the thickness normalized membrane $\hat{A}$ and bending $\hat{D}$ stiffness matrix, together with the laminate thickness h. In addition, the responses are also approximated in terms of the reciprocals of the membrane and bending stiffness matrix. A general approximation form for a response f is written as:

$$\tilde{f} = \sum_{i=1}^{n} \left(\Psi_i^m : \hat{A}_i + \Psi_i^b : D_i + \Phi_i^m : A_i^{-1} + \Phi_i^b : D_i^{-1} + \alpha_i h_i \right) + C_0, \tag{3}$$

where n represents the number of laminates used for response approximation, while the superscripts ^{m} and ^{b} denote respectively, sensitivities with respect to the membrane and bending stiffness matrix. The approximation constant C_0 is calculated based on the response values at the current design point. The operation $\Psi : D = trace(\Psi D)$, is known as matrix contraction, which is composed of matrix multiplication followed by the summation of the diagonal elements. The linear and reciprocal sensitivities of a function f with respect to: membrane and bending stiffness matrix and laminate thickness, are defined as:

$$\Psi^m = \frac{\partial f}{\partial \hat{A}}, \quad \Psi^b = \frac{\partial f}{\partial \hat{D}}, \quad \Phi^m = \frac{\partial f}{\partial \hat{A}^{-1}}, \quad \Phi^b = \frac{\partial f}{\partial \hat{D}^{-1}}, \tag{4}$$

and

$$\alpha = \frac{\partial f}{\partial h}.$$

The accuracy of the response approximation is increased by expressing the approximation as a combination of the linear and reciprocal terms. This however is not possible for all responses, since not all approximations will have the contributions of the linear and reciprocal terms at the same time. Hence, only the terms that provide the most accurate representation of the original response will be considered. It is therefore necessary to have physical insight for all type of responses before formulating their approximate functions. The approximate function, given in equation 4, need to to comply with convexity, separability and conservativeness (Ref. 25).

The current optimization work contains two types of responses; responses derived from the aeroelastic analysis and responses from the high-fidelity structural analysis.

Aeroelastic responses The aeroelastic responses are torque, thrust, power and tip deflection. The first three aeroelastic responses are calculated based on the total aerodynamic force resultant (f_r) and the moment resultant (m_r) calculated at the blade root. The total aerodynamic force and moment resultants are calculated for a hub-height wind speed u as:

$$f_r(u) = \int_0^L f(u,s) J ds$$

and

$$m_r(u) = \int_0^L \left(m(u,s) + r(u,s) \times f(u,s) \right) J ds, \quad (5)$$

where L is the blade length. The aerodynamic force and moment resultants along the blade length are given by f and m respectively. Furthermore, the position vector of the deformed beam axis with respect to the origin of the rotating frame is denoted by r.

Since the aeroelastic analysis is performed for finite (hub-height) wind speeds, the maximum for each aeroelastic response is calculated using the bracketing method. Figure 6 shows a schematic representation of the bracketing scheme to find the maximum of each response. The bracketing scheme

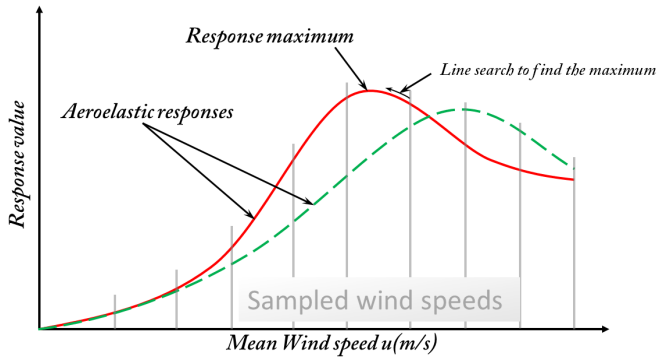

Fig. 6. Bracketing method to find the maximum of the aeroelastic responses

finds the maximum of each response in two steps. First, for a given list of response values, calculated at sampled wind speeds, the wind speed range (u^l, u^u) containing the response maximum is determined. Second, assuming the response curve is convex between (u^l, u^u), the line search method is employed to find the wind speed $\tilde{u} \in [u^l, u^u]$ for which the response has reached its maximum value.

The total torque on the low speed shaft is calculated as:

$$r_{to}(u) = B e_3^t m_r(u), \quad (6)$$

where B refers to the number of blades and $e_3 = \{0,0,1\}^t$.

The total thrust is the sum of the thrusts on all the blades, calculated as:

$$r_{th}(u) = B e_3^t f_r(u), \quad (7)$$

where f_r is the total aerodynamic force on an single blade.

The aerodynamic power is calculated as:

$$P(u) = \omega(u) B e_3^t m_r(u), \quad (8)$$

where ω is the rotational speed.

Since the deformation of the blade resembles the deformation of a cantilever beam, the maximum blade deflection is at the blade tip. Therefore, the maximum blade deflection is given by:

$$\delta_{tip}(u) = \sum_{i=1}^{n} R_{i,p}(\xi = 1) u_i(u), \quad (9)$$

where $R_{i,p}$ is the NURBS function of order p, associated to the control point i. The variable u_i is the displacement vector of the beam axis at control point i.

Structural responses The structural responses are essential in the current optimization framework to size the wind turbine blade. The structural responses consist of stresses of all shell elements (of the finite element model), and the buckling load factors.

Using the stress responses obtained from the static analysis solution by *NASTRAN*, the membrane stress resultants $N = \{N_x, N_y, N_{xy}\}^t$ of element i are given by:

$$N_i = \frac{1}{2} \hat{h}_i \left(\sigma_i^u + \sigma_i^l \right), \quad (10)$$

where $\hat{h}_i$ is the shell thickness of element i and σ_i^u and σ_i^l are the stresses at the upper and lower end of element i. The method of extracting the stress responses σ_i^u and σ_i^l is covered in (Ref. 19).

In addition to the stress responses, *NASTRAN* is also used to calculate the buckling load factor λ_n. *NASTRAN* calculates the buckling load factor based on the equation:

$$\{K + \lambda_n K_d\} \phi_n = 0, \quad (11)$$

where ϕ_n is the mode shape of the buckling load λ_n, whereas K, and K_d are respectively, the stiffness matrix and differential stiffness of the finite element model. The differential stiffness is a function of the geometry and the displacement, where the displacement is a solution of a particular static solution used in the buckling analysis.

Mass The blade mass is also part of the optimization process. It is used to calculate the cost of energy. Furthermore, the blade mass can also be used as an objective function. The blade mass depends on the laminate thickness and its density. The density of all elements is not necessarily the same, because some parts of the blade are made up of sandwich structures (to prevent buckling). The blade mass is calculated as:

$$M = \int_0^L m_0 ds, \quad (12)$$

where L is the blade length and m_0 is the mass per unit length.

Cost Of Energy The cost model described in this section is based on the *NREL* cost model for pitch regulated wind turbines and modified in (Ref. 26) to calculate the Cost Of Energy (*COE*) of stall regulated wind turbines. The *COE* is used to evaluate the optimality of each design iteration that meets the desired criteria. The *COE* is calculated from the expected annual energy production and the cost of each *HAWT* component as:

$$COE = \frac{FCR \times ICC}{AEP_{Net}} + AOE, \tag{13}$$

where *FCR* is the fixed charge rate and *ICC* is the initial capital cost. The net annual energy production AEP_{Net} is defined as:

$$AEP_{Net} = \text{availability} \times \int_{u_{ci}}^{u_{co}} P(u) f_p(u) du, \tag{14}$$

where u_{ci} and u_{co} are the cut-in and cut-out wind speeds respectively, $P(u)$ is the power production as a function of the mean wind speed, and $f_p(u)$ is the probability of occurrence, calculated with the Weibull distribution (Ref. 27). The shape and scale parameters for the Weibull distribution are chosen to match an off-shore wind climate (Ref. 28).

The annual operation expenses, *AOE*, are expressed as:

$$AOE = \frac{OM + LRC}{AEP_{Net}} + LLC, \tag{15}$$

where *OM* are the levelized operation and maintenance costs, *LRC* is the levelized replacement and overhaul cost, and *LCC* is the land lease cost. It is assumed that for stall regulated machines, the pitch mechanism is not used for power regulation, while the component is still used during emergency or parked state of the turbine. Furthermore, the *LLC* is assumed unaffected in current optimization while the remaining components of the *COE* are either dependent on the design variables or on the pith factor. The pitch factor determines the fraction of *OM* and *LRC* compared to the respective cost components of the *NREL 5MW* pitch machine, assuming that the pitch system is not used for power regulation, such that:

$$OM = \beta OM_{ref} \qquad \text{and} \qquad LRC = \beta LRC_{ref} \tag{16}$$

where OM_{ref} and LRC_{ref} are respectively, the levelized operation and maintenance costs and the levelized replacement and overhaul costs of the *NREL5MW* pitch machine, while $\beta \in [0,1]$ is the pitch factor.

During the optimization process, the change in initial capital cost, *ICC*, is calculated from the load overshoots: power, torque and thrust together with the blade mass. The overshoots in power, torque, and thrust are defined as the maximum power, torque, or thrust of the new design divided by its rated equivalent of the *NREL 5MW* pitch machine, i.e.:

$$\psi_i = \frac{r_i}{r_i^{ref}}, \text{ for } i = 1 \ldots 4, \tag{17}$$

where i refers to the type of overshoot. The aeroelastic response of the new design is denoted by r_i, while r_i^{ref} refers, for the same response, the (rated) aeroelastic response of the *NREL 5MW* pitch regulated machine. The *ICC* of each *HAWT* component of the *NREL 5MW* pitch regulated machine is multiplied by the appropriate ψ_i to determine the *ICC* of the new design. Table 1 contains component-wise breakdown of the *ICC* and the design driving load types for the relevant *HAWT* component, which is consistent with the cost model of (Ref. 29). The electrical interface cost is calculated assuming a 7 by 7 array spacing (Ref. 26). Furthermore, it is noted that the initial capital costs of the blades and hub are affected by the blade mass while the blade mass is sized by the structural load types: stress, buckling and Maximum Blade Deflection (MBD). The effect of the structural load types on the *ICC* components is also shown in table 1. The present cost model assumes a fixed rotor radius, resulting in fixed cost for the main bearings, yaw drive and bearings, nose cone, control hardware and marinization.

Table 1. Design driving load types for each HAWT component and breakdown of *ICC* per component

Load Type	*HAWT* components(% of *ICC*)
Stress, Buckling & MBD	Blades(8), Hub(1)
Maximum Torque	Low Speed Shaft(< 1), Gearbox(7), Main Brakes(< 1), Generator(3)
Maximum Power	Power Electronics(4), Electrical Connections(2), Nacelle(< 1), Hydraulics and Cooling(< 1), Electrical Interface(13)
Maximum Thrust	Tower(7), Support Structures(16)

Approximation The response approximations are in general, either in terms of the laminate membrane and bending stiffness matrices or their reciprocal part, together with the laminate thickness. Due to the necessity of the approximation to be convex to ensure a global minimum of the approximate function, reciprocal approximations that are not convex are convexified using the method presented in (Refs. 25, 30). The convexification process introduces a linear term that replaces the non-definite part of the reciprocal term.

For brevity, the sensitivities in the approximation formulation are denoted as Ψ, Φ, and α, irrespective of the response type. Furthermore, the superscripts ^{m} and ^{b} on Ψ and Φ represent respectively, sensitivities with respect to laminate membrane and bending stiffness matrix. The response approximations used in the current optimization study are summarized in table 2, where detailed description on the response approximation is given in (Ref. 19). The subscript j runs over the number of laminates used as design variables.

Table 2. Response approximations

Power	$\tilde{r}^p \simeq \sum_j \Psi_j^m : A_j + \Psi_j^b : D_j + \alpha_j h_j$
Tip deflection	$\tilde{r}^\delta \simeq \sum_j \Phi_j^m : A_j^{-1} + \Psi_j^m : A_j + \Phi_j^b : D_j^{-1} + \Psi_j^b : D_j + \alpha_j h_j$
Strength	$\tilde{r}_i^s \simeq \frac{\partial r_i^s}{\partial A_i^{-1}} : A_i^{-1} + \left(\frac{\partial r_i^s}{\partial N_i}\right)^t \sum_j \Psi_{ij}^m : A_j + \Psi_{ij}^b : D_j + \alpha_{ij} h_j$
Buckling	$\tilde{r}_i^b \simeq \sum_j \Phi_{ij}^m : A_j^{-1} + \Psi_{ij}^m : A_j + \Phi_{ij}^b : D_j^{-1} + \Psi_{ij}^b : D_j + \alpha_{ij} h_j$
Mass	$\tilde{r}^m \simeq \sum_j \alpha_j h_j$
Relative *COE*	$\tilde{r}^c \simeq \sum_j \Psi_j^m : A_j + \Psi_j^b : D_j + \alpha_j h_j$

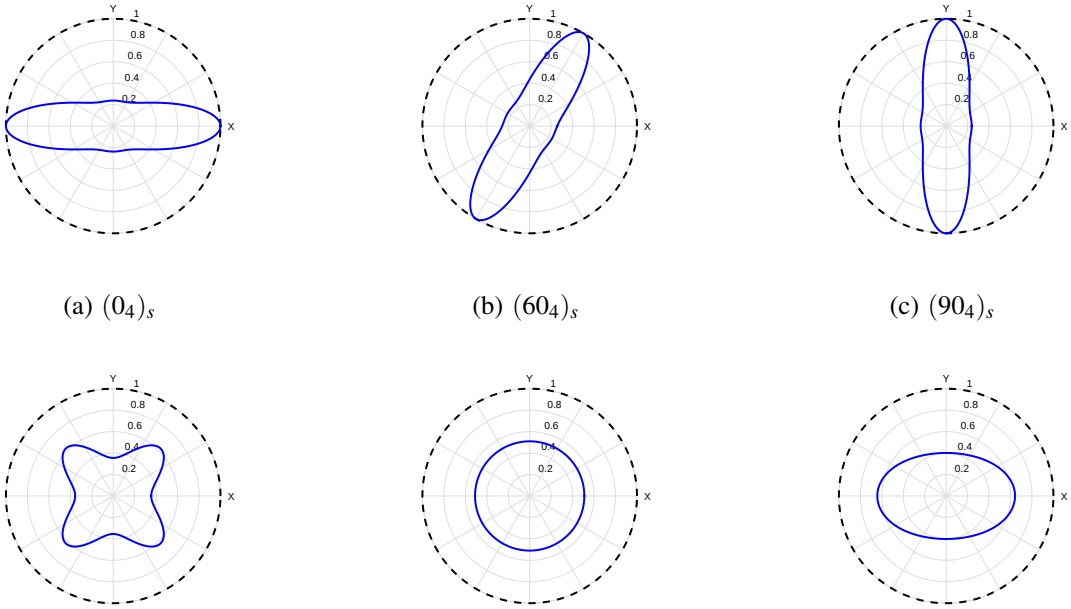

(a) $(0_4)_s$ (b) $(60_4)_s$ (c) $(90_4)_s$

(d) $(\pm 45_2)_s$ (e) $(\pm 45, 0, 90)_s$ (f) $(\pm 45_2, 0_4, 90)_s$

Fig. 7. $\hat{E}_{11}(\theta)$ distribution for various stacking sequence.

MEMBRANE STIFFNESS VISUALIZATION

One of the challenges in stiffness-based optimization is to visualize the stiffness distribution of the design solutions. Particularly, it is difficult to visualize the membrane stiffness matrix (A), since there is no direct link between A and the fiber angles (stacking sequence). In order to visualize the distribution of the in plane stiffness matrix (A), the thickness-normalized engineering modulus of elasticity, $\hat{E}_{11}(\theta)$, for $\theta = 0$ to 360 deg, is calculated using:

$$\hat{E}_{11}(\theta) = \frac{1}{e^t \tilde{A}(\theta) e}, \tag{18}$$

where

$$\tilde{A}(\theta) = T^T \hat{A}^{-1} T, \tag{19}$$

$e^t = \{1,0,0\}$, and $\hat{A}$ is the thickness-normalized membrane stiffness matrix. The variable T is the transformation matrix given by:

$$T = \begin{bmatrix} cos^2\theta & sin^2\theta & 2cos\theta sin\theta \\ sin^2\theta & cos^2\theta & -2cos\theta sin\theta \\ -cos\theta sin\theta & cos\theta sin\theta & cos^2\theta - sin^2\theta \end{bmatrix}. \tag{20}$$

A polar plot of $\hat{E}_{11}(\theta)$ is given in figure 7 for several characteristic laminate sequences. In figure 7, the x axis refers to the 0° fiber angle, while the y axis refers to the 90° fiber angle. The laminate stiffness matrix for the characteristic laminate sequences is generated using the ply properties of table 3. The engineering modulus of elasticity, $\hat{E}_{11}$, of all laminates is normalized with the modulus of elasticity of a single ply (E_{11}). Figure 7(a) shows $\hat{E}_{11}$ of laminate where the fibers are all aligned in x direction, while figure 7(c) shows the engineering modulus of elasticity of a laminate with all the fibers aligned along the y axis. Figure 7(b) shows that all the fibers of the laminate are all aligned 60° with respect to the x axis. The membrane stiffness distribution of a quasi-isotropic laminate is depicted in figure 7(e), where the membrane stiffness is equally distributed in all direction. Finally, figure 7(d) and 7(f) show a polar plot of $\hat{E}_{11}$ for ±45° layup and a semi quasi-isotropic layup, having the majority of the fibers aligned along the x axis.

Table 3. Material properties of a single ply

E_{11}	E_{22}	G_{12}	ν	ρ
35.0e9	8.33e9	4.12e9	0.33	1920

RESULTS

Baseline design

The initial design is based on the *NREL 5MW* blade design (Ref. 31). However, the *NREL 5MW* machine is a pitch regulated machine, thus the choice of airfoils and twist distribution are modified such that the blade is suitable for use in stall controlled machine. The gross properties of the current machine are given in table 4. The chord distribution for the current design is the same as the chord distribution of the *NREL 5MW* blade design. The twist distribution is designed for optimum operation below rated wind speed while inducing sufficient stall for high wind speed, specially at the outboard blade region. Consequently, the twist distribution is calculated using

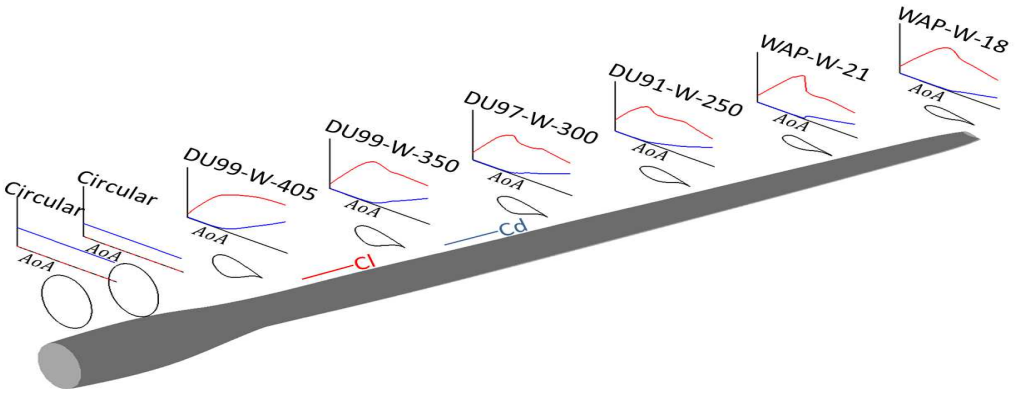

Fig. 8. Blade shape together with the base airfoils and their aerodynamic characteristics.

Table 4. Gross properties for the 5MW baseline wind turbine

Rating	5MW
Rotor orientation, Configuration	Upwind, 3 Blades
Control	Variable Speed, Stall controlled
Rotor, Hub diameter	126 m, 3 m
Hub height	90 m
Cut-in,Rated,Cut-out wind speed	3 m/s, 9 m/s, 25 m/s
Cut-in,Rated rotor speed	6.9 rpm, 10.4 rpm

equation 21, for a tip speed ratio $\lambda = 7.55$, axial induction factor $a = 1/3$, and design angle of attack $\alpha = 10\,\text{deg}$.

$$\theta = \frac{1}{r/R}\frac{1-a}{\lambda} - \alpha, \tag{21}$$

The airfoil shapes, at the blade root and inner region of the blade, are taken from the *NREL 5MW* blade design. The airfoils for the outer region of the blade are obtained from an airfoil design study, geared towards airfoil designs with improved stall characteristics at high Reynolds number ($Re = 9 \times 10^6$) (Ref. 32). Two airfoils are selected for the outer blade region: 21% thick airfoil (WAP-W-21) and 18% thick airfoil (WAP-W-18). The new 21% thick airfoil is employed between 38% and 69% of the blade span, with a maximum of 96% of the 21% airfoil shape realized at 53% of the blade span. The new 18% thick airfoil is employed between 53% of the blade span till the blade tip, where the blade cross-section consists solely of the 18% thick airfoil starting 70% of the blade span. The blade planform is generated using NURBS basis functions of cubic polynomials and 17 control points with which the blade geometry is defined. A 3D representation of the turbine blade and the airfoil distribution together with their 2D aerodynamic characteristics is given in figure 8.

Material properties The material properties across the blade cross-section are assigned by partitioning the cross-section in three sections along the chord (see figure 4). Three laminates define the material properties of the skin on pressure side and three laminates on the suction side. Finally, a single laminate is used to define the material properties of the shear webs. Glass fiber laminates are used to define the material properties of the wind turbine rotor blade. The material properties of the glass fiber laminate, including the strain allowables, are given in table 5. The strain allowables in table 5 already include a safety factor of 2.977, which is a combination of loads and material safety factor (Ref. 33).

Table 5. Material properties selected from (Ref. 33).

Component (material)	**E_{11},GPa**	**E_{22},GPa**	**G_{12},GPa**	**ν**	**ρ,Kg/m^3**
Face-sheet (Glass)	**35**	**8.33**	**4.12**	**0.33**	**1920**
Core (Foam)	**0.256**	**0.256**	**0.022**	**0.3**	**200**
		Allowables			
Component (material)	**ε_t%**		**ε_c%**		**γ_{xy}%**
Face-sheet (Glass)	**0.95**		**0.75**		**0.91**
Core (Foam)	**-**		**-**		**-**

The initial layup consists of quasi-isotropic laminates with the layup $[\pm 45, 90, 0]_s$, where the 0deg is aligned with the blade axis and the subscript s refers to a symmetric laminate. The spar-caps of the rotor blade are composed of conventional laminates, while the remaining structural components of the rotor blade are composed of sandwich laminates. The core of the sandwich laminates consist of foam with the properties of the foam material given in table 5. The ratio of core thickness to the face-sheet thickness (given in table 6) is based on the Sandia rotor blade design (Ref. 34).

Table 6. Ratio of core to face-sheet thickness for a sandwich laminate

R(m)	leading edge	trailing edge	shear web
0	2	2	25
1.4	2	2	25
1.5	2	2	25
6.8	21	21	25
9.0	27	27	25
43.1	7	7	25
45.0	7	7	25
61.5	7	7	25

Optimization model There are 13 design variables per laminate (12 design variables for membrane and bending stiffness of the laminate plus the laminate thickness). The material

properties are defined using 7 laminates across a cross-section (per control point) and 15 control points along the blade span, which amounts to 105 laminates and 1365 design variables.

The aeroelastic loads are calculated for sampled wind speeds between the cut-in and cut-out wind speed. Furthermore, the aeroelastic loads calculated at wind speeds above rated are used as load cases for the stress and buckling analysis using the finite element solver *NASTRAN*. The responses considered are: stress, buckling, tip deflection, rated power, blade mass, and CoE, where the CoE is used as the objective function. The finite element solver *NASTRAN* provides stress responses together with buckling load factors. The strain failure indices, based on the stress responses of the *NASTRAN* analysis, are formulated using a conservative failure envelope (Ref. 25). The strain failure envelope is constructed using the strain allowables of glass fiber, listed in table 5.

In order to present the stiffness distribution of a blade design, a polar plot is used to visualize the in-plane stiffness distribution of the laminates along the blade span, using equation 18. For the laminate stiffness distribution of the initial design, a polar plot of the thickness-normalized engineering modulus of elasticity (on the suction side of the blade skin and shear webs) is given in figure 9. The x direction of the material coordinate system (0deg) is indicated by the black line, which for a straight blade is aligned with the beam axis. Looking at figure 9 , the laminate stiffness distribution is the same in every direction, suggesting a quasi-isotropic laminates. The blade skin on the pressure side has the same stiffness distribution.

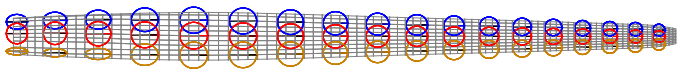

(a) Blade skin on suction side

(b) shear webs

Fig. 9. Stiffness distribution for the initial design.

Design studies of twist coupled turbine blade: COE minimization

The benefit of unbalanced laminates over balanced laminates to design adaptive blades with improved performance is investigated. The performance of different blade designs is assessed using optimization scheme that minimizes the COE of stall regulated wind turbines while complying with structural and aeroelastic constraints. A complete stiffness variation along the blade span is considered during the optimization. Both balanced and unbalanced composite laminates are investigated during the optimization, while ensuring no structural and aeroelastic failure (strain, buckling, and tip displacement). Furthermore, additional optimization studies are performed with an additional constraint on the maximum power, to determine the capability of twist coupled blades to regulate power on stall controlled wind turbines. The results are verified using different starting designs for the optimization cases, comprised of different laminate thickness and stiffness distribution.

The results of COE and it's components, for all design solutions, are normalized with the corresponding values of the *NREL 5MW* pitch controlled machine, shown in table 7. In addition, the same *OM* and *LRC* (cost components of the COE) value as for the reference NREL 5MW pitch regulated machine is assumed in the current optimization, resulting in conservative estimation of the COE for all designs.

Table 7. Performance of the NREL 5MW pitch regulated machine

COE	**AEP**	**ICC**	**Mass**
$\$/Kwh$	Kwh	$\$$	Kg
0.082	$\mathbf{2.4}\times10^{7}$	$\mathbf{1.1}\times10^{7}$	$\mathbf{17.7}\times10^{3}$
Power$_{rated}$	**Torque**$_{rated}$	**Thrust**$_{rated}$	**Tip displacement**
MW	Nm	N	m
5.3	$\mathbf{4.2}\times10^{6}$	$\mathbf{7.1}\times10^{5}$	**5**

Balanced vs Unbalanced laminates

The first performance comparison is between balanced and unbalanced laminate design solutions. Both balanced and unbalanced laminates are used separately to minimize the COE of stall regulated wind turbine. Up-wind configuration is adopted for both cases, meaning the tip displacement is constrained together with the structural constraints (strain & buckling). First, the optimization is carried out for the balanced laminates using the initial design as starting point. The staring design for the optimization using unbalanced laminates is the final design from the optimization case using balanced laminates. Therefore, since the unbalanced design contains the balanced design as a special case, it seems that the solutions are local optima. Table 8 shows the cost components

Table 8. Cost components of balanced and unbalanced design solutions. The results are normalized with the corresponding values of the *NREL 5MW* pitch regulated machine.

Laminate type	COE	AEP	ICC	Blade mass
Balanced	1.11	1.08	1.29	1.34
Unbalanced	1.09	1.06	1.25	1.30

of the balanced and unbalanced designs. The results are normalized with the corresponding values of the *NREL 5MW* pith regulated machine. According to table 8, design solution with unbalanced laminates reduced the blade mass and therefore the ICC. The reduction in blade mass is due to the reduced lift, which is caused by increase in angle of attack. This however will reduce the annual energy production. The net result

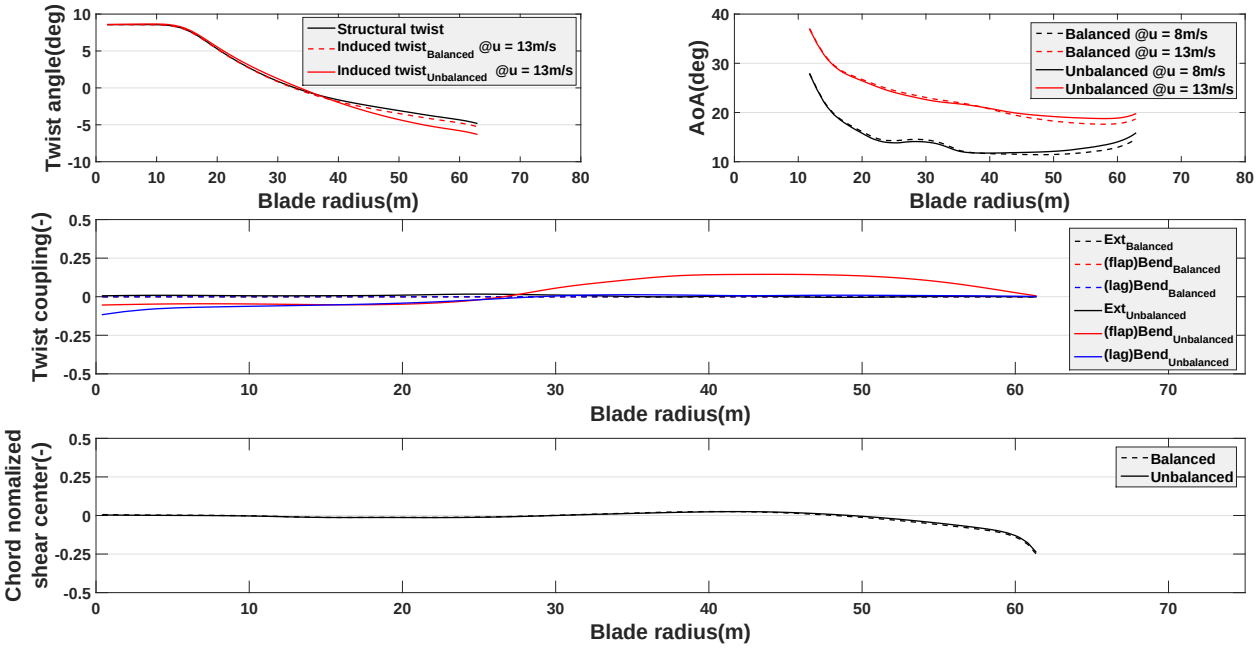

Fig. 10. Span-wise variation of: twist angle, angle of attack, twist-coupling, and location of shear center for balanced and unbalanced design solutions.

on the cost of energy is that a 2% reduction in COE is observed for the design using unbalanced laminates compared to the balanced laminates.

The turbine performance given in table 8 can be understood by looking at figure 10. The reduction in AEP and blade mass is due to a different *induced* twist distribution for the final design compared to the initial design (see top left plot of figure 10). The term *induced* refers to the twist distribution due to the aeroelastic response of the blade, which can be controlled by changing the extension-twist or bend-twist coupling of the blade or the location of the shear center. From the top left plot of figure 10, it is observed that the *induced* twist for the balanced design (dashed red line) moves slightly towards stall (increased angle of attack) compared to the structural twist (solid black line), especially towards the outboard region of the blade. For the design using unbalanced laminates (solid red line), the *induced* twist moves significantly towards stall (increased angle of attack) for the outboard blade region, with a maximum difference of 1.5deg compared to the structural twist. For the unbalanced design however, the induced twist shifts slightly towards feather for the inboard blade region between 20% to 35% of blade radius. The *induced* twist has a clear influence on the angle of attack (see the top right window of figure 10). For the design with unbalanced laminates, a larger increase in angle of attack for the outboard blade region is observed (solid line), compared to the design using balanced laminates (dashed line). The legend of the middle plot of figure 10 represent: (*Ext*) extension-twist coupling, ((*flap*)*Bend*) flap-wise bend-twist coupling and ((*lag*)*Bend*) lag-wise bend-twist coupling. The different twist coupling coefficients of figure 10 are calculated according to,

$$ext = \frac{S_{14}}{\sqrt{S_{11}S_{44}}},\ bend_{flap} = \frac{S_{54}}{\sqrt{S_{55}S_{44}}},\ \text{and}$$
$$bend_{lag} = \frac{S_{64}}{\sqrt{S_{66}S_{44}}}, \quad (22)$$

where the S_{ij} are the coefficients of a sectional stiffness constant of a the turbine blade. According to figure 10, the change in *induced* twist for the design with balanced laminates is not due to twist coupling but rather due to a shift in the shear center. The twist coupling plot shows zero coupling terms for the balanced laminates (dashed lines) and significant twist coupling for the design with unbalanced laminates (solid lines). The shear center is a point on a cross-sectional plane, through which the application of a transverse load does not cause twist moment (see figure 11). The location of the shear center is calculated from the sectional stiffness constants as:

$$e = -\frac{S_{34}}{S_{44}}. \quad (23)$$

According to figure 11, moving the shear center back towards the trailing edge increases the *induced* twist towards stall, while moving it towards the leading edge shifts the *induced* twist towards feather. Looking at the bottom window of figure 10 , the location of the shear center, for both designs, has moved towards the trailing edge, especially towards the outboard blade region. The shift of the shear center towards the trailing edge causes the *induced* twist to reduce towards stall (see the top left window of figure 10). The location of the shear center is controlled by the redistribution of the laminate thickness across the cross-section. Since balanced laminates

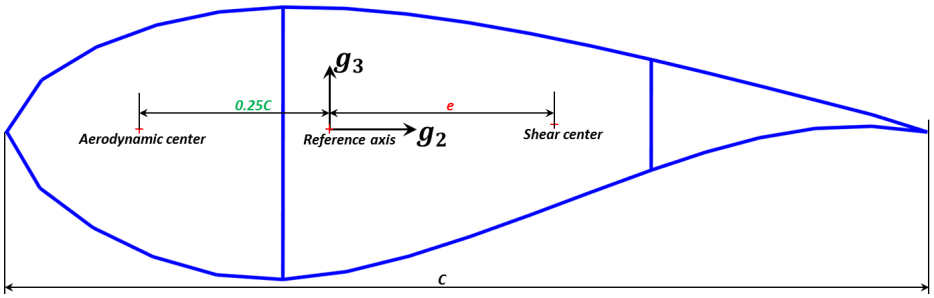

Fig. 11. Schematic representation of shear center and aerodynamic center on a cross-sectional plane

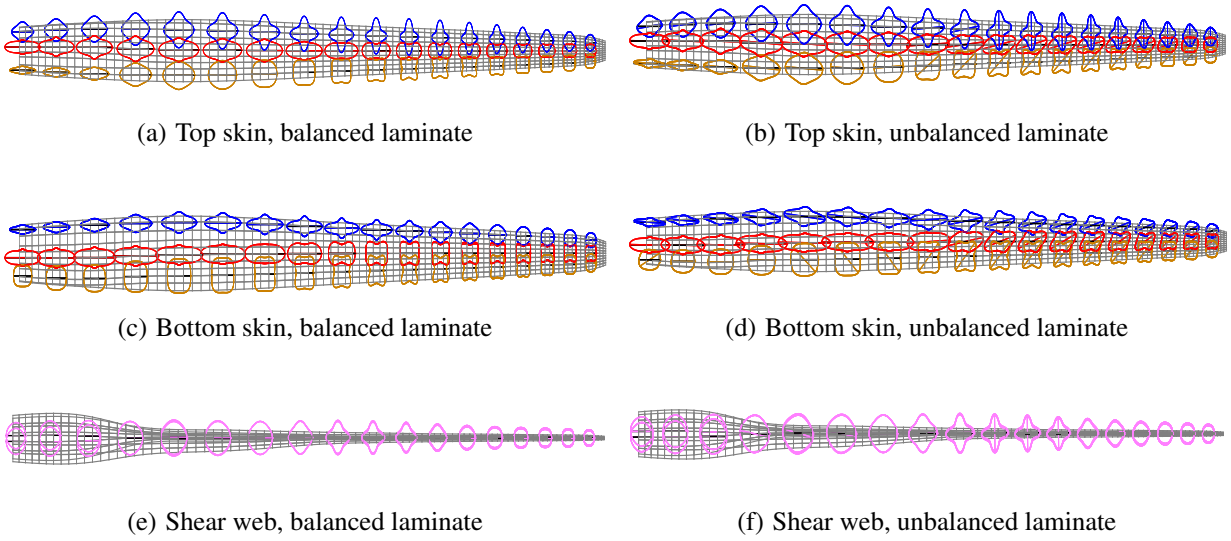

(a) Top skin, balanced laminate

(b) Top skin, unbalanced laminate

(c) Bottom skin, balanced laminate

(d) Bottom skin, unbalanced laminate

(e) Shear web, balanced laminate

(f) Shear web, unbalanced laminate

Fig. 12. $\hat{E}_{11}$ of optimized stiffness distribution for balanced and unbalanced laminates.

can't induce bend-twist or extension-twist coupling, the optimizer shifts the *induced* twist towards stall by moving the location of the shear center towards the trailing edge.

For the design solution with unbalanced laminates, the change in *induced* twist is mostly attributed to the twist coupling (see the middle window of figure 10). The flap-wise bend-twist coupling starts with negative coupling coefficient and changes sign roughly at the blade midspan, almost the same location where the *induced* twist changes direction, i.e. changes from twisting towards feather to twisting towards stall. Furthermore, negative value for flap-wise bend-twist coupling is observed for the inboard blade region, twisting the inboard region of the blade towards feather. There is almost no extension twist coupling for both design solutions.

The difference in twist coupling for the balanced and unbalanced design is best explained by figure 12. Figure 12 shows a polar plot of the thickness normalized engineering modulus ($\hat{E}_{11}$), for both balanced and unbalanced designs. The figure contains the major stiffness direction on the top and bottom skin and the shear webs. The black line inside the polar plots represents the material x direction, which is aligned with the beam axis. For the balanced design, the stiffness distribution of all laminates is symmetric with respect to the black line, inducing no twist coupling. Most of the laminate stiffness for the inboard blade region, especially towards the blade root, are all aligned along the material direction, providing structural strength (mainly buckling). For the outboard region, the stiffness direction for the leading edge laminates (brown curves) is around the angle $\pm 45^\circ$, while for the trailing edge laminates (blue curves), the stiffness direction for the same span-wise location is towards the 90°. The stiffness direction of the spar cap laminates (red curves) is aligned with the blade axis for the inner blade region and rotates roughly to $\pm 45^\circ$ close to the blade tip. The stiffness direction of the shear web laminates, around the mid section of the blade span, are rotated to 90° with respect to the blade axis. Furthermore, stiffness distribution of the shear web laminates is the same for both design solutions.For the unbalanced laminates, most of the stiffness direction on both sides of the blade skin are rotated clockwise(inboard region) and counter-clockwise (outboard region) with respect to the material x direction (black line), inducing (flap-wise) bend-twist coupling shown in figure 12. The laminate stiffness distribution for the shear webs is mostly quasi-isotropic, except roughly between 30% to 45% of the blade span, where the major stiffness direction is rotated to 90° with respect to the beam axis. Finally, the effect of induced twist on

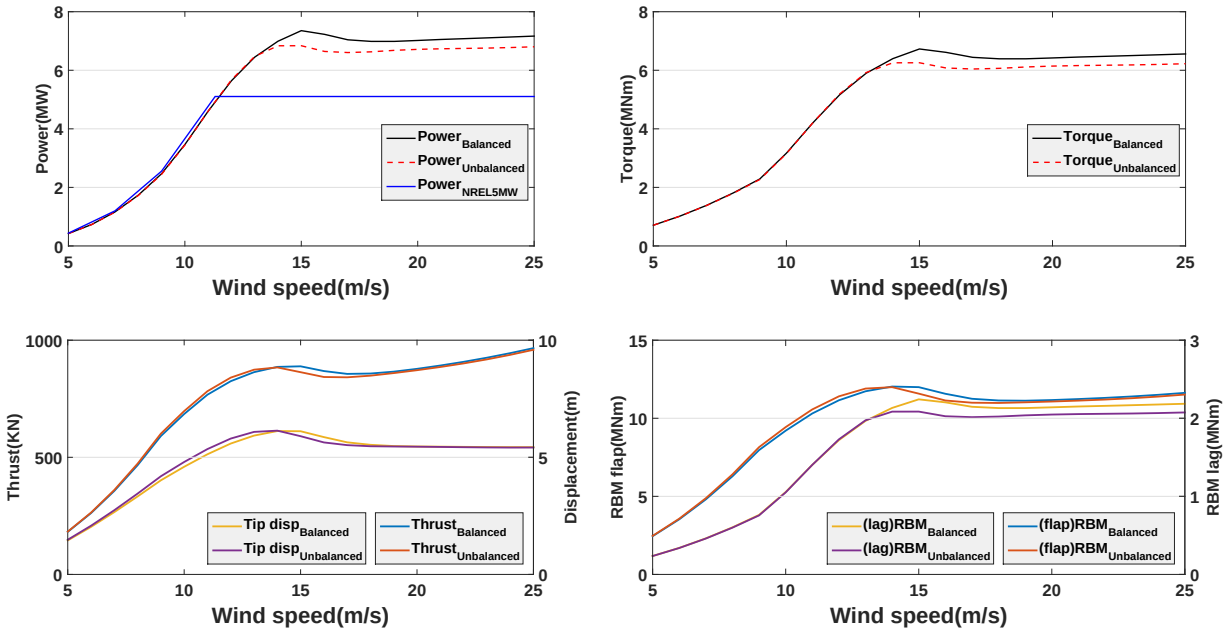

Fig. 13. Aeroelastic response (power, torque, root bending moment, and tip displacement) for balanced and unbalanced design solutions.

the aerodynamic performance of the wind turbine is shown in figure 13. The top left window of figure 13 presents the power curves for the balanced and unbalanced designs together with the power curve of the *NREL 5MW* pitch controlled machine. Increased angle of attack reduces the maximum power, as shown in figure 13. The same reduction in rated torque is also observed for the unbalanced design (see the top right window of figure 13). However, only slight reduction in thrust and flap-wise root bending moment is observed for the unbalanced design compared to the balanced design (see bottom left and right windows of figure 13).

Constrained power

Furthermore, two optimization cases are carried out with an additional constraint on maximum power and using only unbalanced laminates as design variables. The constraint on maximum power is set to 110% and 120% of the rated power of the NREL 5MW pitch machine. Besides the constraint on maximum power, structural constraints (strain and buckling) together with the constraint on tip displacement are included in the optimization. The starting design for both cases is the final design from the optimization using balanced laminates. Table 9 shows the cost components of the final design, where the listed values are normalized with the corresponding value of the NREL 5MW pitch controlled machine, given in table 7. From table 9, the COE seems to increase the stringent the constraint on maximum power becomes. The same trend is also observed for the AEP and blade mass, while the ICC decreases for more stringent constraint on maximum power. Furthermore, it is observed that the constraint on maximum power is active for power overshoots less than 1.3 of the rated

Table 9. Cost components of the final design for different constraint on maximum power. The results are normalized with the corresponding values of the *NREL 5MW* pitch regulated machine.

					Load overshoots		
Constrained Power	COE	AEP	ICC	Blade mass	Power	Torque	Thrust
1.10	1.13	0.97	1.20	1.62	1.10	1.40	1.34
1.20	1.11	1.02	1.24	1.58	1.20	1.52	1.34
Unconstrained	1.09	1.06	1.25	1.30	1.30	1.65	1.35

power of the NREL pitch controlled machine. The twist coupling of the final designs is shown in figure 14, which contains the distribution of the three twist coupling modes (extension, flap-wise bend, and lag-wise bend) along the blade axis. The solid black curves are for the design with a constraint on power equal to 110% of the NREL 5MW pitch controlled machine. The dashed red lines correspond to the design with 120% constraint on maximum power. Finally, the dotted blue lines are for the design with no constraint on maximum power.

It is observed that a significant extension-twist coupling is present for the final designs with a constraint on maximum power. However, the extension-twist coupling for the design with no constraint on power is negligible compared to the other designs. Significant flap-wise bend-twist coupling is achieved for all the design cases, where positive coupling coefficient (throughout the blade span) is obtained only for the design with the most stringent constraint on maximum power. A positive lag-wise bend-twist coupling coefficient is observed only for designs that include a constraint on maximum power, while for the unconstrained design (in-terms of power), the coupling coefficient is mostly negative.

Furthermore, the top right window of figure 14 shows the ra-

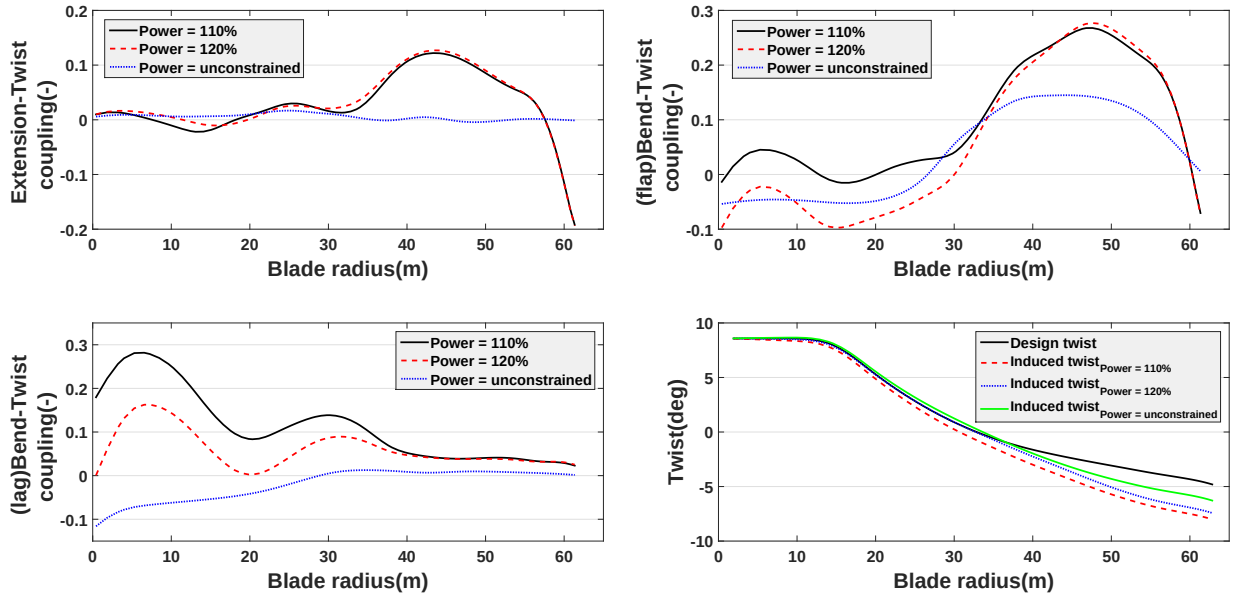

Fig. 14. Twist coupling and induced twist, for different constraint on maximum power.

dial variation of the *induced* twist coupling for the different designs. The black line with the label *design* twist refers to the initial twist distribution. As expected, the lowest *induced* twist is for the design with power constraint of 110%, having a maximum reduction in twist by 3 deg (with respect to the *design* twist). Furthermore, a maximum difference of 2.5deg in twist is observed for the design with power constraint of 120%.

As a result of lower *induced* twist coupling, a lower power curve is obtained (see figure 15). Figure 15 contains the power curve of the optimized designs with a different level of constraints on maximum power. Furthermore, figure 15 also contains the power curve of the NREL 5MW pitch controlled machine. The maximum power tends to decrease for more stringent constraint on power. However, it comes at the cost of reduced power for lower (below rated) wind speeds. This is also observed in lower annual energy production (AEP), as shown in table 9.

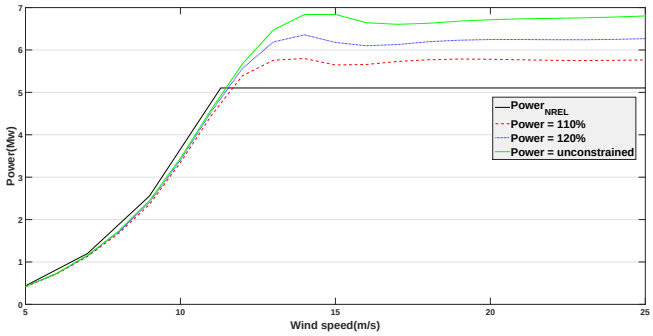

Fig. 15. Power curve for different constraint on maximum power.

CONCLUSIONS

This paper presents an optimization framework to improve the performance of wind turbine rotor blades using variable stiffness composite laminates. The potential of twist coupled blades to regulate the power on stall controlled wind turbines is investigated by exploiting the characteristic of unbalanced laminates to induce twist coupling. A complete stiffness variation along the blade span is considered during the optimization. The results are verified using different starting designs for the optimization cases, where the different starting designs are comprised of different thickness and stiffness distribution.

The cost of energy is used as an objective function during the optimization, while considering both structural and aerodynamic constraints. It should be noted that the present cost model is only a simplified first order approximation of the COE based on the COE of *NREL 5MW* pitch regulated machine , provided that the load overshoots for the new design are not large (≤ 1.5). For larger load overshoots, the linearisation of the ICC in terms of the load overshoots is not accurate and a more elaborated cost model needs to be formulated. In addition, the same *OM* and *LRC* value as for the reference *NREL 5MW* pitch machine are assumed in the current optimization, resulting in a conservative estimation of the COE for all designs. Therefore, the present cost model serves only to provide a first order estimate of the direction into which the COE might go during stiffness optimization of stall regulated wind turbine blades. Hence, only the relative difference in COE between different design solutions is of interest in this study.

Design solution with unbalanced laminates reduced the blade mass and therefore the ICC. The reduction in blade mass is due to the reduced lift, which is caused by increase in angle of attack. This however will reduce the annual energy pro-

duction. The net result on the cost of energy is that a 2% reduction in COE is observed for the design using unbalanced laminates compared to the balanced laminates. The change in the aerodynamic performance of the wind turbine is due to a shift of *induced* twist distribution(towards stall) for the unbalanced laminates compared to the *induced* twist distribution of balanced laminates. Compared to the *design* twist, a maximum difference in twist angle of $\approx$ 1.5deg is achieved for unbalanced laminates while for balanced laminates the difference is less than $\approx$ 0.5deg. The difference is mainly due to the twist coupling (both extension-twist and bend-twist) which are zero for balanced laminates while for unbalanced laminates, a maximum (flap-wise) bend-twist coupling coefficient of 0.14 is achieved. However, the final design with unbalanced laminates showed no significant extension-twist coupling. The shift in the location of the shear center(towards the trailing edge) is the mechanism that the design solution with balanced laminates uses to achieve a reduction of $\approx$ 0.5deg in *induced* twist. The shift in the location of the shear center is achieved by redistributing the laminate thickness across the cross-section, specially on the outer part of the blade. Furthermore, the main stiffness direction for the design with balanced laminates is symmetric with respect to the blade axis, while for the unbalanced laminates, the major stiffness direction is rotated to the right (20 to 30deg) with respect to the beam axis, providing the aforementioned bend-twist coupling coefficient of 0.14.

An optimization study is also carried out with additional constraint on maximum power. Two optimization cases are carried out to minimize the COE with different level of constraint on the maximum power. The results show that the COE and blade mass increase for more stringent constraint on maximum power. On the other hand, the AEP and ICC decreases as the constraint on maximum power becomes more stringent. Furthermore, the AEP deceases steeper than the ICC as the constraint on maximum power becomes more stringent. This is mainly due to the accumulative effect of the load overshoots on the ICC, dominating the direction in which the COE goes during the optimization. It is also observed that the constraint on maximum power is active for power overshoots lower than 130% of the rated power of the *NREL 5MW* pitch regulated machine. This indicates that a linear approximation of the ICC in-terms of the load overshoots lowers the fidelity of the present cost model, and a higher order approximation of the ICC in-terms of the load overshoots is needed.

REFERENCES

[1]Lobitz, D. W., Veers, P. S., Eisler, G. R., Laino, D. J., Migliore, P. G., and Bir, G., *The use of twist-coupled blades to enhance the performance of horizontal axis wind turbines*, Sandia National Laboratories, 2001.

[2]Karaolis, N., Mussgrove, P., and Jeronimidis, G., "Active and passive aeroelastic power control using asymmetric fibre reinforced laminates for wind turbine blades," Proceedings of the 10th British Wind Energy Conference, London, 1988.

[3]Kooijman, H., *Bending-torsion coupling of a wind turbine rotor blade*, Netherlands Energy Research Foundation ECN, 1996.

[4]Ong, C.-H. and Tsai, S. W., *Design, manufacture and testing of a bend-twist D-spar*, Sandia National Laboratories, 1999.

[5]De Goeij, W., Van Tooren, M., and Beukers, A., "Implementation of bending-torsion coupling in the design of a wind-turbine rotor-blade," *Applied Energy*, Vol. 63, (3), 1999, pp. 191–207.

[6]Lobitz, D. W., Veers, P. S., and Laino, D. J., "Performance of twist-coupled blades on variable speed rotors," Technical report, Sandia National Labs., Albuquerque, NM (US); Sandia National Labs., Livermore, CA (US), 1999.

[7]Maheri, A., Noroozi, S., and Vinney, J., "Application of combined analytical/FEA coupled aero-structure simulation in design of wind turbine adaptive blades," *Renewable Energy*, Vol. 32, (12), 2007, pp. 2011–2018.

[8]Maheri, A., Noroozi, S., and Vinney, J., "Decoupled aerodynamic and structural design of wind turbine adaptive blades," *Renewable Energy*, Vol. 32, (10), 2007, pp. 1753–1767.

[9]Capuzzi, M., Pirrera, A., and Weaver, P., "A novel adaptive blade concept for large-scale wind turbines. Part I: Aeroelastic behaviour," *Energy*, Vol. 73, 2014, pp. 15–24.

[10]Capuzzi, M., Pirrera, A., and Weaver, P., "A novel adaptive blade concept for large-scale wind turbines. Part II: Structural design and power performance," *Energy*, Vol. 73, 2014, pp. 25–32.

[11]Capuzzi, M., Pirrera, A., and Weaver, P., "Structural design of a novel aeroelastically tailored wind turbine blade," *Thin-Walled Structures*, Vol. 95, 2015, pp. 7–15.

[12]Bottasso, C., Campagnolo, F., Croce, A., and Tibaldi, C., "Optimization-based study of bend–twist coupled rotor blades for passive and integrated passive/active load alleviation," *Wind Energy*, Vol. 16, (8), 2013, pp. 1149–1166.

[13]Hayat, K. and Ha, S. K., "Load mitigation of wind turbine blade by aeroelastic tailoring via unbalanced laminates composites," *Composite Structures*, Vol. 128, 2015, pp. 122–133.

[14]Zuteck, M. D., *Adaptive blade concept assessment: curved planform induced twist investigation*, Citeseer, 2002.

[15]Ashwill, T. D., "Sweep-twist adaptive rotor blade: final project report." Technical report, Sandia National Laboratories, 2010.

[16]Ferede, E., Abdalla, M. M., and van Bussel, G. J., "Isogeometric based framework for aeroelastic wind turbine blade analysis," *Wind Energy*, Vol. 20, (2), 2017, pp. 193–210.

[17]Cottrell, J. A., Hughes, T. J., and Bazilevs, Y., *Isogeometric analysis: toward integration of CAD and FEA*, John Wiley & Sons, 2009.

[18]Piegl, L. A. and Tiller, W., *The NURBS book*, Springer, 1995.

[19]Ferede, E., *Static Aeroelastic Optimization of Composite Wind Turbine Blades using Variable Stiffness Laminates*, TU Delft, Delft University of Technology, 2016.

[20]Jelenić, G. and Crisfield, M., "Geometrically exact 3D beam theory: implementation of a strain-invariant finite element for statics and dynamics," *Computer Methods in Applied Mechanics and Engineering*, Vol. 171, (1), 1999, pp. 141–171.

[21]Crisfield, M. A. and Jelenić, G., "Objectivity of strain measures in the geometrically exact three-dimensional beam theory and its finite-element implementation," *Proceedings of the Royal Society of London. Series A: Mathematical, Physical and Engineering Sciences*, Vol. 455, (1983), 1999, pp. 1125–1147.

[22]Ferede, E. A. and Abdalla, M. M., "Cross-sectional modelling of thin-walled composite beams," Proceedings of the 55th AIAA/ASMe/ASCE/AHS/SC Structures, Structural Dynamics, and Materials Conference, 2014.

[23]Burton, T., Sharpe, D., Jenkins, N., and Bossanyi, E., *Wind energy handbook*, John Wiley & Sons, 2001.

[24]Shen, W. Z., Mikkelsen, R., Sørensen, J. N., and Bak, C., "Tip loss corrections for wind turbine computations," *Wind Energy*, Vol. 8, (4), 2005, pp. 457–475.

[25]IJsselmuiden, S. T., *Optimal design of variable stiffness composite structures using lamination parameters*, TU Delft, Delft University of Technology, 2011.

[26]Pereira, R., Ferede, E., van Bussel, G., and Timmer, W., "Planform Optimization of Active Stall Controlled HAWT rotor," *Submitted to Wind Energy Journal*, 2015.

[27]Hennessey Jr, J. P., "Some aspects of wind power statistics," *Journal of applied meteorology*, Vol. 16, (2), 1977, pp. 119–128.

[28]Morgan, E. C., Lackner, M., Vogel, R. M., and Baise, L. G., "Probability distributions for offshore wind speeds," *Energy Conversion and Management*, Vol. 52, (1), 2011, pp. 15–26.

[29]Fingersh, L. J., Hand, M. M., and Laxson, A. S., "Wind turbine design cost and scaling model," , 2006.

[30]Dillinger, J. K. S., *Static Aeroelastic Optimization of Composite Wings with Variable Stiffness Laminates*, TU Delft, Delft University of Technology, 2014.

[31]Jonkman, J. M., Butterfield, S., Musial, W., and Scott, G., *Definition of a 5-MW reference wind turbine for offshore system development*, National Renewable Energy Laboratory Golden, CO, 2009.

[32]Batlle, E. C., Pereira, R., Kotsonis, M., and de Oliveira, G., "Airfoil Optimisation for DBD Plasma Actuator in a Wind Energy Environment: Design and Experimental Study," 55th AIAA Aerospace Sciences Meeting, 2017.

[33]Griffith, D. T. and Ashwill, T. D., "The Sandia 100-meter all-glass baseline wind turbine blade: SNL100-00," *Sandia National Laboratories, Albuquerque, Report No. SAND2011-3779*, 2011.

[34]Resor, B. R., "Definition of a 5MW/61.5 m wind turbine blade reference model," *Albuquerque, New Mexico, USA, Sandia National Laboratories, SAND2013-2569 2013*, 2013.